



PERGAMON



Atmospheric Environment 35 (2001) 1111–1122

ATMOSPHERIC
ENVIRONMENT

www.elsevier.com/locate/atmosenv

Variability in ultraviolet total optical depth during the Southern California Ozone Study (SCOS97)

Laurent Vuilleumier^{a,*}, Robert A. Harley^b, Nancy J. Brown^a, James R. Slusser^c, Donald Kolinski^{1,c}, David S. Bigelow^c

^aEnvironmental Energy Technologies Division, Lawrence Berkeley National Laboratory, 1 Cyclotron Road, Berkeley, CA 94720, USA

^bCivil and Environmental Engineering Department, University of California, Berkeley, CA 94720, USA

^cNatural Resource Ecology Laboratory, Colorado State University, CO, USA

Received 12 July 1999; received in revised form 10 April 2000; accepted 24 April 2000

Abstract

Formation of photochemical air pollution is governed in part by the solar ultraviolet actinic radiation flux, but wavelength-resolved measurements of UV radiation in polluted urban atmospheres are rarely available. As part of the 1997 Southern California Ozone Study, cosine weighted solar irradiance was measured continuously at seven UV wavelengths (300, 306, 312, 318, 326, 333 and 368 nm) at two sites during the period 1 July to 1 November 1997. The first site was at Riverside (260 m a.s.l.) in the Los Angeles metropolitan area, which frequently experiences severe air pollution episodes. The second site was at Mt Wilson (1725 m a.s.l.), approximately 70 km northwest of Riverside, and located above much of the urban haze layer. Measurements of direct (i.e., total minus diffuse) solar irradiance were used to compute total atmospheric optical depths. At 300 nm, optical depths (mean \pm 1 S.D.) measured over the entire study period were 4.3 ± 0.3 at Riverside and 3.7 ± 0.2 at Mt Wilson. Optical depth decreased with increasing wavelength, falling at 368 nm to values of 0.8 ± 0.2 at Riverside and 0.5 ± 0.1 at Mt Wilson. At all wavelengths, both the mean and the relative standard deviation of optical depths were larger at Riverside than at Mt Wilson. At 300 nm, the difference between the smallest and largest observed optical depths corresponds to over a factor 2 increase in the direct beam irradiance for overhead sun, and over a factor 7 increase for a solar zenith angle of 60° . Principal component analysis was used to reveal underlying factors contributing to variability in optical depths. PCA showed that a single factor (component) was responsible for the major part of the variability. At Riverside, the first component was responsible for 97% of the variability and the second component for 2%. At Mt Wilson, 89% of the variability could be attributed to the first component and 10% to the second. Dependence of the component contributions on wavelength allowed identification of probable physical causes: the first component is linked to light scattering and absorption by atmospheric aerosols, and the second component is linked to light absorption by ozone. These factors are expected to contribute to temporal and spatial variability in solar actinic flux and photodissociation rates of species including ozone, nitrogen dioxide, and formaldehyde. © 2001 Elsevier Science Ltd. All rights reserved.

Keywords: Sun photometry; Optical depth; Variability; Aerosol; Principal Component Analysis

1. Introduction

Photochemical air pollution problems persist in many urban and regional environments, despite ongoing efforts to control precursor emissions. While gas-to-particle conversion processes have received considerable attention in recent years (e.g., Odum et al., 1997; Meng et al.,

* Corresponding author. Tel.: +1-510-486-6108; fax: +1-510-486-7303.

E-mail address: L_Vuilleumier@lbl.gov (L. Vuilleumier).

¹Now with University Corporation for Atmospheric Research (UCAR), Boulder, CO, USA.

1997), less is known about reverse interactions such as how aerosols interact with solar ultraviolet radiation to affect photochemical reaction rates in the atmospheric boundary layer. Dickerson et al. (1997) present measurements and model predictions showing that UV-scattering particles (e.g., sulfate aerosol) in the boundary layer can enhance smog formation, whereas UV-absorbing aerosols (e.g., soot) decrease ozone formation. Furthermore, a number of sensitivity studies (for example, Falls et al., 1979; Milford et al., 1992; Gao et al., 1995, 1996; Yang et al., 1995, 1996; Vuilleumier et al., 1997; Bergin et al., 1998) have examined the sensitivity of ozone production to various chemical reactions, and have identified the photolysis of nitrogen dioxide (NO_2) and formaldehyde (HCHO) as being among the most important.

A large-scale field study of ozone formation in Southern California (SCOS97-NARSTO) was conducted during summer 1997, to improve understanding of the emissions, atmospheric chemistry, and meteorological conditions leading to the notorious photochemical air pollution problems in the Los Angeles area. Our focus in this paper is the analysis of solar UV irradiance measurements made at two Southern California sites experiencing different levels of air pollution. Photochemical reactions depend on the solar actinic flux while solar irradiance is the quantity measured in this study. Actinic flux and solar irradiance are related by a geometric factor, i.e., the irradiance is weighted by the cosine of the incident zenith angle, while the actinic flux is not. The relationship between actinic flux and irradiance can be complex, and is an active area of research. For more details the reader is referred to Madronich (1987) who describes the relationship between these two quantities in detail.

Our research has as its long-term goal to improve the treatment of actinic flux for simulating photochemistry in air quality models. Our initial efforts have been concerned with quantifying the variability of actinic flux. We have analyzed ground-based UV irradiance data from the SCOS97 field campaign at Riverside and Mt Wilson, California. We have computed total optical depths (i.e., the solar direct beam differential extinction rate per unit of vertical path length, see Section 2.1) and determined their distribution for the period extending from July to the end of October 1997. We also computed the correlation coefficients between pairs of optical depths measured at different wavelengths, and used principal component analysis (PCA) to identify the underlying factors responsible for the variability observed in the optical depths. If this variability is accounted for in the calculation of actinic flux, the uncertainty in photolysis rates in air quality models can be reduced and our calculation of ozone formation improved. Principal component analysis allows us to attribute the optical depth variability mainly to concentration changes in aerosols and marginally to changes in the ozone column.

In Section 2, we describe how the irradiance data were acquired, and explain the algorithm used to obtain total optical depths from the irradiance. We also specify the selection criteria that were applied to the data set, and discuss the optical depth distributions. In Section 3, we present the statistical methods that were used to analyze optical depth variability. We show how correlation coefficients were obtained from the optical depth distributions, and how PCA was applied to identify underlying factors responsible for the optical depth variability. The results of the statistical analysis are discussed at the end of Section 3. Finally, we conclude by summarizing our findings and presenting some avenues of research that could be pursued in future studies.

2. SCOS97 data

2.1. Experimental measurement

The irradiance data used in this study were acquired during the 1997 Southern California Ozone Study (SCOS97) at two sites selected for intensive monitoring. The first site is at Riverside, CA (260 m a.s.l., latitude 33.94°N , longitude 117.40°W) in the Los Angeles metropolitan area, and is characterized by frequent occurrences of severe air pollution episodes. The second site is Mt Wilson, CA (1725 m a.s.l., latitude 34.23°N , longitude 118.07°W) approximately 70 km northwest of Riverside, a mountainous site located above much of the urban haze layer. The measurement period extended from 1 July to 1 November 1997.

Solar UV irradiance reaching the ground was measured at seven wavelengths by two prototype Yankee Environmental Systems (Turners Falls, MA) UV multi-filter rotating shadow-band radiometers (MFRSR) (Bigelow and Slusser, 2000) SN 231 at Riverside and 232 at Mt Wilson. These radiometers have 2 nm nominal full-width at half-maximum filters whose center wavelengths are 300.4, 305.7, 312.0, 318.1, 325.9, 332.9 and 367.8 nm. Bigelow et al. (1998) have shown that integrated out-of-band light contamination is less than 0.5%. A shadow-band blocks the direct solar beam to yield diffuse horizontal irradiance, which is subtracted from the total horizontal irradiance to give direct horizontal irradiance. In order to obtain absolute measurements of the solar irradiance, calibration factors should be used. However, optical depth can be computed using uncalibrated relative irradiances (see below). From this point, we will use the term “irradiance” to refer to the uncalibrated quantity. The direct normal solar irradiance used for computing total optical depths is obtained by dividing the direct horizontal irradiance by the cosine of the solar zenith angle and then applying angular corrections previously measured in the laboratory (Harrison and Michalsky, 1994). Measurements at the seven wave-lengths were

made simultaneously every 20 s and nine such measurements were averaged to form a 3-min average. The averaged data were stored in a data logger until transferred by modem to the Colorado State University data facility each night.

Total optical depths were deduced from the irradiance data. The optical depth is part of the exponent of the Beer–Lambert–Bouguer law

$$I(t) = R^2 I_0 \exp\left(-\sum_i m_i(t)\tau_i(t)\right)$$

$$\rightarrow \ln(R^2 I_0) - \ln(I(t)) = \sum_i m_i(t)\tau_i(t), \quad (1)$$

where $I(t)$ is the direct normal solar irradiance at time t (I_0 is the extra-terrestrial irradiance), R is the Earth-to-Sun distance in astronomical units, and m_i and τ_i are the optical mass factors and optical depths for the different light-absorbing and scattering materials in the atmosphere (Rayleigh, ozone, aerosol, etc.). The expression in Eq. (1) is often approximated with (see Schotland and Lea, 1986)

$$\ln(R^2 I_0) - \ln(I(t)) = m_e(t)\tau(t) \quad \text{with } m_e(t) = \frac{\sum_i m_i(t)\tau_i(t)}{\sum_i \tau_i(t)}, \quad (2)$$

where $m_e(t)$ is the effective air mass factor, and $\tau(t)$ is the total optical depth. When the value of $\ln(R^2 I_0)$ is known, an instantaneous total optical depth can be computed for each individual direct irradiance measurement. Values need not be known with an absolute calibration, but need to be known only relatively. If $V(t)$ is the radiometer reading (in mV) corresponding to the measurement $I(t)$, one needs only to know the value V_0 corresponding to $R^2 I_0$ to calculate the instantaneous total optical depth

$$\tau(t) = \frac{\ln V_0 - \ln V(t)}{m_e(t)}. \quad (3)$$

Absolute calibrations were not available for the prototype UV multifilter radiometers used in SCOS97. Thus, the Langley plot method (see Slusser et al., 2000) was used to determine the $\ln V_0$ intercept. The direct normal solar irradiance data measured during a 2–4 h period was expressed as a function of the air mass factor traversed by the direct solar beam. The time period were chosen such that the air mass factor ranged from 1.2 to 2.2 at the shorter wavelengths (300, 306, and 312 nm), and from 1.5 to 3 at the longer wavelengths. The $\ln V_0$ intercept was obtained by extrapolating a linear regression of the logarithm of irradiance as a function of air mass factor to the zero air mass axis. The Harrison and Michalsky algorithm (1994) was used to select periods for which the Langley method was applicable. Two modifications were made to the Harrison and Michalsky algorithm: 1) the air mass factor ranges are different (see above);

2) Harrison and Michalsky requested that the standard deviation or $\ln I$ around the regression line be less than 0.006, while we used 0.0009. This method has been evaluated in numerous publications via intercomparisons to other optical depth measuring devices beginning with Harrison and Michalsky's original objective algorithm paper and most recently in an intercomparison of four solar radiometers at the ARM site in Oklahoma (Schmid et al., 1999). It has been extended to UV wavelengths by numerous researchers including Bigelow and Slusser (2000) and Slusser et al. (2000).

Computation of the optical depths and $\ln V_0$ intercepts requires the effective air mass factor $m_e(t)$ to be known. For computing $m_e(t)$, one needs to know at every desired time, the optical mass factors and optical depths for all materials responsible for light extinction in the atmosphere. Missing this information, we replaced $m_e(t)$ by the air mass factor due to Rayleigh scattering $m_R(t)$. These terms (m_e and m_R) are different because of the difference in elevation profiles of the light-absorbing and scattering materials in the atmosphere, and replacing one by the other introduces a bias. These differences have been discussed extensively in the literature (e.g., Thomason et al., 1983 or Tomasi et al., 1998). The elevation profile of ozone is one of the profiles that differs most from the profile of the uniformly mixed atmospheric gases that is used for evaluating Rayleigh scattering. To estimate an upper limit on the bias that was introduced when replacing $m_e(t)$ by $m_R(t)$, we computed it assuming only ozone and uniformly mixed atmospheric gases, a 300 DU total ozone column, and a standard atmosphere with a sea-level pressure of 1013 hPa. At Mt Wilson and Riverside, the bias in the optical depth is less than 2% at $\lambda = 300$ nm, and for $m_R = 2$, considering the effect of replacing $m_e(t)$ by $m_R(t)$ in Eq. 2 and in the determination of $\ln V_0$. At all other wavelengths the bias is smaller, since ozone has a weaker influence at higher wavelengths.

For each wavelength and site, the average $\ln V_0$ values were applied to all days assuming that the variations in extraterrestrial irradiance (I_0) were negligible,² and that the instruments were stable. In order to test these assumptions, the distributions and time series for $\ln V_0$ were analyzed. A downward trend with time was visible in the time series for some wavelengths and sites (for example, see Fig. 1a). Linear regressions were computed for each time series. When the linear correlation coefficient (r) was greater than 1/3 (in absolute value) the downward trend was characterized as significant and the linear regression was used to compensate for it. In cases where the trend is significant ($|r| > 1/3$), the value of the regression line for the desired time is used instead of the

² The spectral irradiance of the sun between 300 and 400 nm is constant within 0.5% over an 11-year solar cycle (Lean et al., 1997).

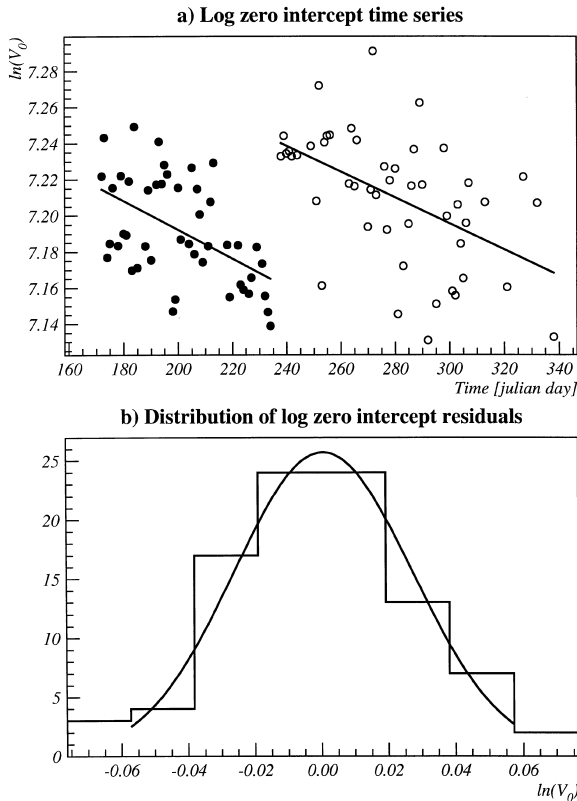


Fig. 1. Logarithm of zero intercept ($\ln V_0$) time series and residual distribution for Mt Wilson at $\lambda = 333$ nm. V_0 is the value in mV that would be obtained by measuring the extraterrestrial irradiance with the radiometer used in this study.

average $\ln V_0$. Bigelow and Slusser (2000) and Slusser et al. (2000) also observed a similar drift with the same type of radiometer. Bigelow and Slusser are unsure of the cause of this minor drift. A noticeable feature occurs for the $\ln V_0$ time series for data taken at Mt Wilson. When a trend is significant at Mt Wilson, the time series are split in two distinct groups with a recovery around Julian day 234. On this day, the Mt Wilson radiometer was moved because of concerns about the original location.

The distributions of the residuals between the individual values of $\ln V_0$ and the regression line (significant trend) or the average (insignificant trend) were used to check the quality of the determination of $\ln V_0$. When the number of residuals is sufficient (larger than 60), a Gaussian can be fitted to describe the residual distribution (see Fig. 1b). For each case with more than 60 residuals, the data look consistent with a normal distribution. The uncertainty on $\ln V_0$ can be computed using the residual distributions providing the following assumptions are true.

(1) The uncertainty in the determination of $\ln V_0$ comes from the variability in the atmospheric conditions and not from the instability of the detector.

(2) The uncertainty is statistically distributed with a normal distribution around the true value of $\ln V_0$.

The first assumption is warranted because the multifilter shadowband radiometers are stable, and random variations due to the instruments are negligible compared to variation in atmospheric optical properties (Bigelow and Slusser, 2000). The second assumption is warranted since all residual distributions with more than 60 events are compatible with a normal distribution. Thus, a 95% confidence level interval u can be computed for $\ln V_0$,

$$\overline{\ln V_0} - u \leq \ln V_0 \leq \overline{\ln V_0} + u, u = t_{0.25} \frac{s'}{\sqrt{n}} \quad (4)$$

at 95% confidence level,

where $\overline{\ln V_0}$ is the average $\ln V_0$ or the value obtained with linear regression, $t_{0.25}$ is the critical value at a 95% confidence level for the Student–Fisher T -distribution, s' is the estimator of the variance of the residual distribution and n is the number of residuals.

Having established the precision for $\ln V_0$, it is interesting to evaluate the relative uncertainty in τ_i ,

$$\frac{\sigma(\tau_i)}{\tau_i} = \frac{\sqrt{\sigma^2(\ln V_0) + \sigma^2(\ln V_i)}}{(\ln V_0 - \ln V_i)} \quad (5)$$

The uncertainty of $\ln V_0$ depends on the wavelength. At wavelengths where the optical depth is usually small (longer wavelengths), it is also less variable. Consequently, the Langley plot method for determining $\ln V_0$ is more precise and the uncertainty is reduced. At short wavelengths, especially at 300 nm, the Langley plot method is more difficult to apply and the uncertainty in $\ln V_0$ is large. However, at the shorter wavelengths, the large optical depth results in a large difference ($\ln V_0 - \ln V_i$) that compensates for the large uncertainty in $\ln V_0$. Hence, the relative uncertainty of τ_i is of the same order at all wavelengths.

For each wavelength and each site, an upper limit was estimated for the relative τ_i uncertainty considering only the contribution from $\ln V_0$ uncertainty. For this purpose, the 95% confidence interval and the smallest measured difference ($\ln V_0 - \ln V_i$), i.e., the worst case, was used. At Riverside, this estimation was on the order of 5% at 300 and 368 nm, and lower at all other wavelengths. At Mt Wilson, it was of the order of 2% at 300 and 368 nm, and lower at all other wavelengths.

Some uncertainty in τ_i is also due to uncertainty in the direct irradiance measurement. The dominant uncertainty in $\ln V_i$ is due to electronic noise that is of the order of 1 mV. In order to achieve a low relative uncertainty only direct irradiance measurements greater than 50 mV were used in this analysis. Sources of systematical uncertainties other than the bias due to differences in elevation profile of the atmospheric absorbing and scattering material are believed to be negligible (Schmid et al., 1998).

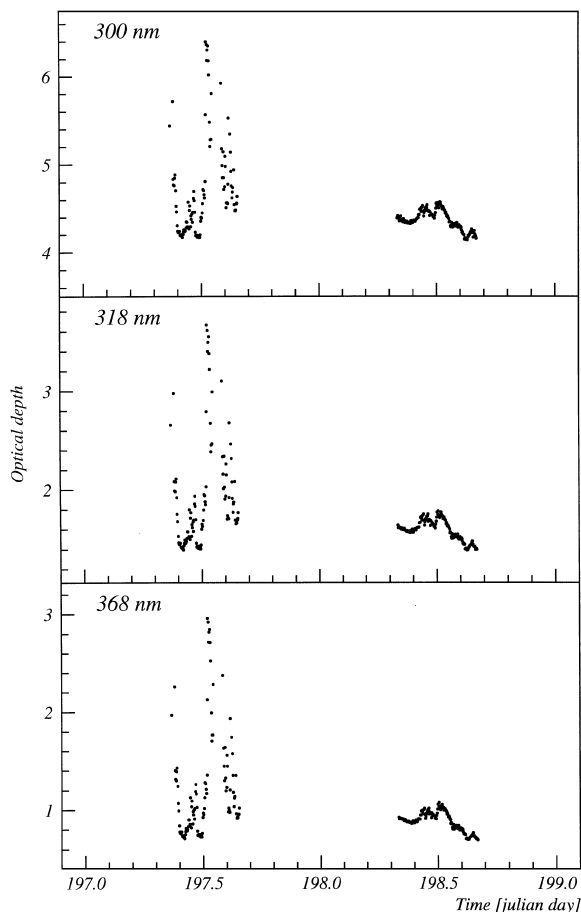


Fig. 2. Optical depth time series for 16 and 17 July 1997 at Riverside at $\lambda = 300, 318$ and 368 nm.

2.2. Cloud influence

When studying optical depth variability, it is important to determine whether clouds are present or not. While in clear sky situations the total optical depth can vary due to absorbing gases and aerosols in the atmosphere, clouds produce such large and rapid optical depth variations that other effects frequently becomes negligible in comparison. Fig. 2 shows the optical depth time series for 16 and 17 July, 1997 at Riverside at wavelength 300, 318 and 368 nm. 16 July is a day when clouds were present, whereas skies were clear on 17 July. On 16 July, the optical depth increased by more than 2 at all wavelengths, in less than an hour, just after midday (Julian day time equal to 197.5). This reflects the localized nature of clouds. In some cases, when clouds are present but not in the direct beam path, the total irradiance may be higher than clear-sky irradiance because of increased diffuse light, while minutes later, the presence of a cloud in the beam path can greatly reduces the total irradiance. On 17 July, optical depth variations were much smaller and slower.

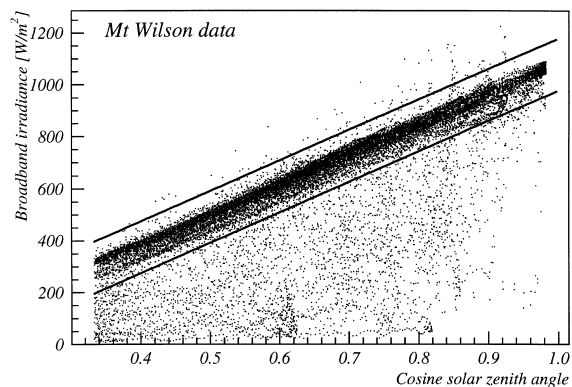


Fig. 3. Broadband visible total solar irradiance vs. cosine solar zenith angle.

In many instances, photochemical air pollution is linked to stagnant high-pressure systems. Because our long-term goal is to improve the treatment of actinic flux for simulating photochemistry in air quality models, we chose to study the optical depth variability for clear-sky situations. During SCOS97, broadband solar irradiance was measured at Riverside and Mt Wilson with Eppley precision spectral pyranometers (PSP). Data were recorded almost continuously during the 4-month measurement period with a frequency between 3 and 15 min. For clear-sky conditions, broadband total solar irradiance depends linearly on the cosine of the solar zenith angle when the latter is below 70° . The broadband irradiance (PSP) data were used to establish the appropriate linear relationship, and the data points for which the irradiance differed by more than 100 W m^{-2} from the established relationship were classified as cloudy periods. The Mt Wilson broadband irradiance data for zenith angle less than 70° are shown in Fig. 3 with the $\pm 100 \text{ W m}^{-2}$ limits.

Clear-sky total optical depths were calculated after rejecting all measurements taken within 30 min (before or after) of cloudy periods. This criterion excludes data similar to those from Riverside on 16 July, and retains data such as those recorded on 17 July (see Fig. 2).

2.3. Distributions of optical depths

The original UV spectral irradiance data set includes 19,568 3-min average measurements of the direct irradiance at each of the seven wavelengths at Riverside and 21,972 measurements at Mt Wilson. After selecting only time periods where the direct irradiance measurement was greater than 50 mV at all wavelengths and rejecting measurements taken at times when clouds were present, it was possible to compute 8232 total optical depths for Riverside and 11,261 for Mt Wilson. As a consequence of the selection criteria, all measurements used in the

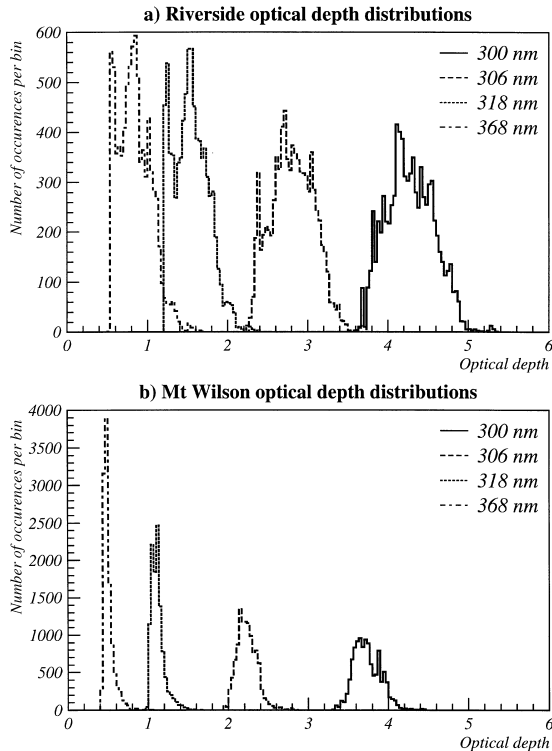


Fig. 4. Optical depth distributions at $\lambda = 300, 306, 317$ and 368 nm.

analysis were made at times when the solar zenith angle was less than 60° , for both sites.

Distributions of optical depths were compiled for both Riverside and Mt Wilson for all wavelengths. Histograms of the distributions at both locations at four wavelengths are shown in Fig. 4. A summary of the optical depth distribution characteristics is shown in Fig. 5 where average values of the optical depth are plotted as a function of wavelength at both sites, and a bar is included to represent the standard deviation.

The optical depths range from about 0.5 (Mt Wilson at $\lambda = 368$ nm) to about 4.3 (Riverside at $\lambda = 300$ nm). At Riverside, the difference between the maximum and minimum for each optical depth distribution is on the order of 1 or larger. This range illustrates the temporal variability in optical depths observed at a single site and wavelength. For a given time, direct beam irradiances for total optical depths τ_1 and τ_2 will differ by a factor $\exp((\tau_1 - \tau_2)A)$. This is more than a factor of 2 for an optical depth difference of 1 with overhead sun ($A = 1$ when the solar zenith angle is zero) and a factor larger than 7 for $A = 2$ (solar zenith angle of 60°). The diffuse irradiance will also be different but the factor must be calculated using a radiative transfer model. The optical depths and the width of their distributions are smaller at

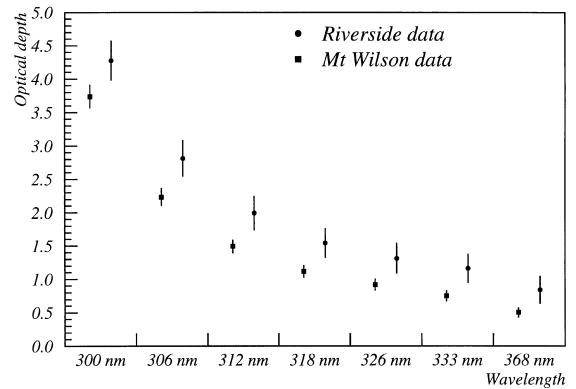


Fig. 5. Averages and standard deviations of the optical depth distributions vs. wavelength.

Mt Wilson. In a pristine environment, these differences would be expected to be the result of spatial and elevational differences. However, the increment in optical depth added by a purely Rayleigh scattering atmosphere accounting for the difference in elevation between Riverside (radiometer 260 m a.s.l.) and Mt Wilson (radiometer 1725 m a.s.l.) is smaller than the observed difference at all 7 wavelengths. A calculation following the formula given by Stephens (1994) yields an optical depth difference of 0.19 at 300 nm and 0.08 at 368 nm, while the observed average differences are 0.54 and 0.34, respectively. The remainder of the difference between the averages in Riverside and Mt Wilson is due to the more polluted air in Riverside that results in greater light absorption and scattering by pollutants. Similarly, the larger variability in Riverside is due to the larger pollution concentration changes observed at Riverside compared to Mt Wilson.

The optical depth decreases as wavelength increases, for the range of wavelengths considered here. The same trend is observed at both Riverside and Mt Wilson. A large decrease in optical depth is observed between 300 and 306 nm, and between 306 and 312 nm. At longer wavelengths, the rate at which optical depth decreases with increasing wavelength is lower. At the wavelengths of our measurements, the optical depths are largely due to absorption and/or scattering by ozone and aerosols because:

- (1) Ozone is an influential light absorbing gas at wavelengths shorter than 330 nm, and its absorption cross section exhibits a sharp drop above 300 nm (Seinfeld and Pandis, 1997, pp. 143–146).
- (2) Aerosols in the atmosphere are known to have broad absorption and scattering cross sections at UV wavelengths, due to the particle size distribution and variability in chemical composition (Seinfeld and Pandis, 1997, pp. 1126–1146).

Analysis of atmospheric composition and visibility in Los Angeles on relatively clean and smoggy days (Larson et al., 1984) has shown that large values of the extinction coefficient (b_{ext}) are mainly due to large amounts of aerosol with diameter ranging from 200 to 500 nm. For UV wavelengths in the same range, the optical depth is expected to vary approximately as $\lambda^{-\nu+2}$ with ν between 2 and 4 (Shaw et al., 1973).

3. Statistical analysis

3.1. Methodology

Our analysis of the optical depth distributions is based on the hypothesis that absorption and scattering by ozone and aerosols are responsible for most of the observed variability. Principal component analysis is a tool of choice to examine this hypothesis and *quantify* the apportionment of the variability among the different factors. PCA is a statistical tool that has been used extensively in environmental sciences. Examples of its use are the apportionment of pollutants to possible sources (e.g., Henry and Hidy, 1979, 1982; Baldasano et al., 1998), and solving inverse problems such as determining the characteristics of light-absorbing and scattering pollutants given the absorption spectrum (Steele and Turco, 1997). PCA is a technique for analyzing the variability of a group of simultaneously measured variables using their correlations (Everitt and Dunn, 1992). The goal of PCA is to uncover the underlying independent factors responsible for the variability observed in the group of variables, and to determine the most influential factors. To achieve this goal, the covariance matrix is diagonalized and expressed as

$$\mathbf{C} = \mathbf{Z} \cdot \mathbf{D} \cdot \mathbf{Z}^{-1}, \quad (6)$$

where \mathbf{C} is the covariance matrix, \mathbf{D} is the diagonalized form, and \mathbf{Z} is the matrix of a rotation operator that transforms the n -dimensional space defined by the variables of interest (n is the number of variables) into a space where the covariance matrix is diagonal. The elements of the diagonal matrix \mathbf{D} are the eigenvalues of \mathbf{C} , and the matrix \mathbf{Z} is formed from the eigenvectors of \mathbf{C} (the i th column of \mathbf{Z} is the eigenvector associated with the i th eigenvalue in \mathbf{D}).

When applying PCA to our data, every simultaneous measurement of the optical depths at the seven wavelengths is considered as a point in the seven-dimensional space. The coordinates of such points are the optical depths measured at each of the wavelengths. The unitary matrix \mathbf{Z} transforms the reference frame of the seven-dimensional space. The components, i.e. the coordinate of each measurement point expressed in the new reference frame, are independent of each other

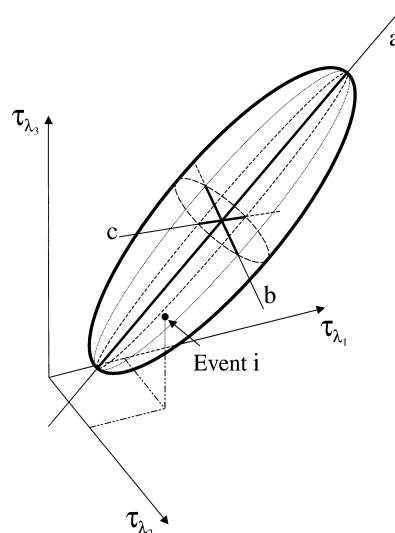


Fig. 6. Geometrical analogy for principal component analysis.

(because the correlation matrix is diagonal in the new reference frame). The first component is chosen so that the largest possible part of the variability occurs along it, the second component so that the largest possible part of the remaining variability occurs along it, etc. It is useful to use a geometrical analogy to understand this approach. Let us assume optical depths are given at only 3 wavelengths, and the points representing the measurements are distributed in an ellipsoid-shaped cluster as shown in Fig. 6. The PCA approach is equivalent to finding a rotation that will align the first component with the longest axis of the ellipsoid (a), and the second component with the second longest axis (b), etc. The elements of the diagonal matrix \mathbf{D} , the eigenvalues of the correlation matrix, are used to determine the relative amount of variability associated with each component. The components define a new reference frame where the covariance matrix is diagonal. Hence, the components are uncorrelated. Determining the alignment of the components in the original reference frame helps identify the components. For this study, when a component makes a very small angle with one axis of the original frame, the underlying factor associated with the component absorbs and/or scatters at the wavelength associated with the axis, but not at the other wavelengths considered. When the angles between one component and all axes of the original reference frame are similar, the underlying factor affects all wavelengths similarly.

3.2. Results

Figs. 7 and 8 show the optical depths for Riverside and Mt Wilson, respectively. The measurements at $\lambda = 300$,

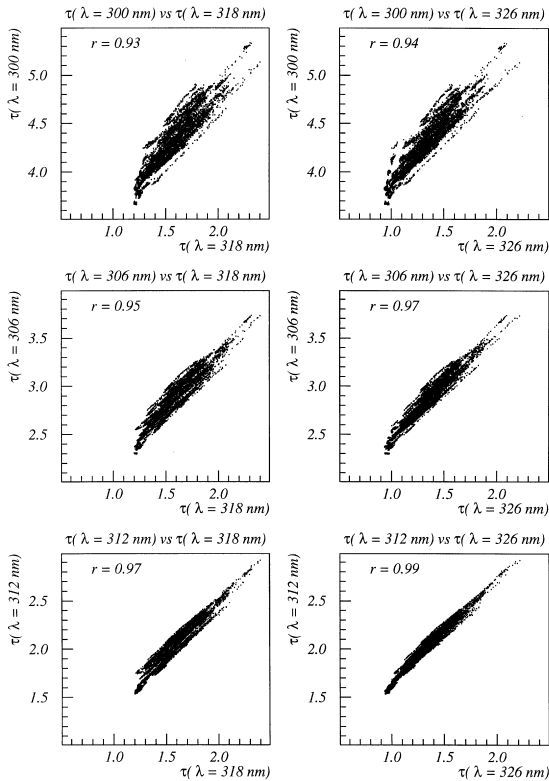


Fig. 7. Optical depth correlations at Riverside (optical depths at 300, 306 and 312 nm vs. optical depths at 318 and 326 nm).

306 and 312 nm are plotted against the measurements at $\lambda = 318$ and 326 nm. The correlation coefficients are included in the figures. Correlations are given instead of covariance because they are normalized and more easily interpreted, whereas covariance can have arbitrarily high values, depending on the variances of the two variables of interest. Similar correlation coefficients were computed for optical depths at all pairs of wavelengths and are given in Table 1.

At Riverside, the main characteristic is the strength of the correlation between measurements at all wavelengths. The weakest correlation coefficient is 0.92. Not surprisingly, correlation tends to be stronger for neighboring wavelengths (close to the diagonal) than for wavelengths that are further apart (away from the diagonal). Exceptions are the correlations between measurements at $\lambda = 318$ nm and smaller wavelengths (third column of the correlation matrix in Table 1) that are weaker than correlations between measurements at 326 nm and smaller wavelengths (fourth column). A possible explanation is that the channel at 318 nm may have had greater measurement noise than the other channels.

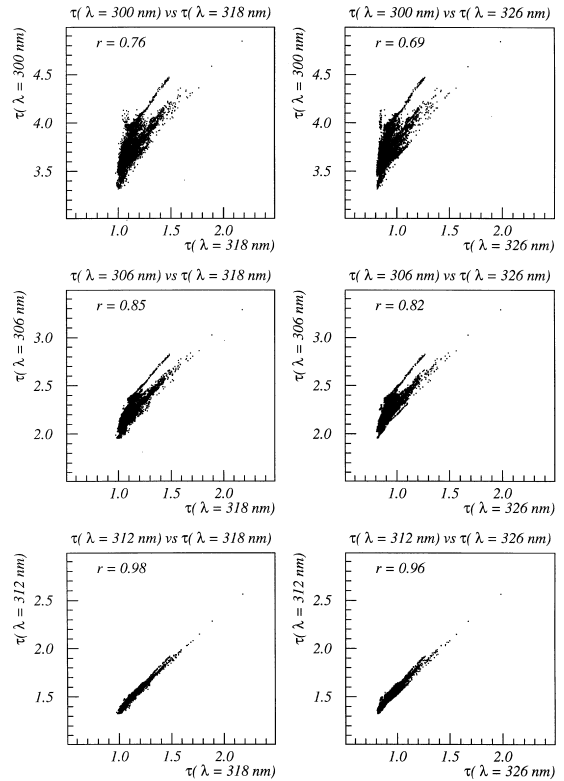


Fig. 8. Optical depth correlations at Mt Wilson (optical depths at 300, 306 and 312 nm vs. optical depths at 318 and 326 nm).

At Mt Wilson, the same overall characteristics of strong correlation with weaker correlation away from the diagonal are observed. However, correlation coefficients are smaller than for Riverside and an additional feature can be distinguished. The correlation between measurements at 300 and 306 nm is strong (0.94), as well as the correlation between measurements at wavelengths longer than 310 nm (four bottom rows of the correlation matrix in Table 1). However, the correlation between measurements at 300 or 306 nm, and measurements at longer wavelengths is weaker. For instance, the correlation between measurements at 300 and 312 nm (0.85) is weaker than the correlation between 312 and 368 nm. This is due to the influence of both aerosols and ozone at 300 and 306 nm, while only aerosols have an influence at longer wavelengths. Similarly, the stronger correlations observed at Riverside than at Mt Wilson is due to a larger influence of aerosols on the optical depths at Riverside (frequent pollution episodes occur at this site).

The eigenvalues of the correlation matrices for Riverside and Mt Wilson are shown in Fig. 9. At Riverside, 97% of the variability is associated with the first component and 2% with the second. At Mt Wilson, the

Table 1
Correlations between optical depth measurements at various wavelengths

Riverside	306 nm	312 nm	318 nm	326 nm	333 nm	368 nm
300 nm	0.99	0.97	0.93	0.94	0.92	0.92
306 nm		0.99	0.95	0.97	0.95	0.95
312 nm			0.97	0.99	0.97	0.97
318 nm				0.99	1.00	0.99
326 nm					1.00	0.99
333 nm						1.00
Mt Wilson	306 nm	312 nm	318 nm	326 nm	333 nm	368 nm
300 nm	0.94	0.85	0.76	0.69	0.62	0.59
306 nm		0.92	0.85	0.82	0.77	0.74
312 nm			0.98	0.96	0.93	0.91
318 nm				0.98	0.96	0.95
326 nm					0.99	0.98
333 nm						1.00

variability associated with the first and second components is 89 and 10%, respectively. While all the components are necessary to explain all the observed variability, a smaller number is sufficient to provide an adequate summary. Rules of thumb to choose the number of components to retain are (Everitt and Dunn, 1992)

1. Include just enough components to explain a relatively large percentage of the total variation (e.g., 90%).
2. Exclude components that have eigenvalues less than a given cut-off value (0.7 has been suggested by Jolliffe, 1972).
3. On a plot of eigenvalues (Fig. 9), locate the point where an “elbow” is present and discard the components after this point.

These rules of thumb suggest selecting only the first component in Riverside, and the two first components at Mt Wilson. For consistency, the two first components are analyzed both for Riverside and Mt Wilson. The matrix \mathbf{Z} can be used to determine the contributions of the optical depths at various wavelengths to the components or, in other words, the angles between the components and the axis of the original reference frame. Figs. 10(a) and (b) indicate the contributions of the various wavelengths to the first and second principal components. Since correlations are used, values are normalized, and the maximum possible contribution is 1. The contributions of all wavelengths to the first component are almost equal, especially for Riverside. Therefore, if the value of the factor responsible for the first component varies, all optical depths will vary in a similar way. The structure of the second principal component reflect the facts that correlation tends to be stronger for neighboring wavelengths than for wavelengths that are further apart. More attention should be devoted to the second

component contributions at Mt Wilson than Riverside, since the second component accounts for only 2% of the variability at Riverside. At Mt Wilson, the largest contribution in absolute value is at $\lambda = 300$ nm, and the contribution at $\lambda = 306$ nm is also strong. At 312, 318 and 326 nm the contribution are weak while they are of the order of 0.35 at 333 and 368 nm. If contributions would all be strictly equal, they would be equal to $\sqrt{1/7}$ or 0.38. When a contribution is below this limit in absolute value, the corresponding component has little influence at the corresponding wavelength. When it is above, the component has a strong influence at this wavelength. Since the contribution is significantly stronger at 300 nm, the second component has its strongest influence at this wavelength. At Riverside a similar behavior is observed, although the anomaly pointed out for the correlations at 318 nm shows up in the second component.

Given a priori knowledge about the absorbing properties of ozone and aerosols in the atmosphere, the interpretation of the principal component analysis is relatively straightforward. The first component, explaining most of the data variability, and corresponding to simultaneous increases or decreases of the optical depth at all observed wavelengths, is linked to the presence of aerosols that absorb and scatter light over the full range of wavelengths measured. The second component that distinguishes between the shorter and longer wavelengths and has a stronger association with the absorption at $\lambda = 300$ nm is linked to ozone whose absorption spectrum declines sharply at wavelengths longer than 300 nm. “Contamination” of the components might occur, giving rise to measurement error contributions to the first or second component, or ozone contributions to the first component and aerosol contributions to the second. However, the remarkable similarity between the

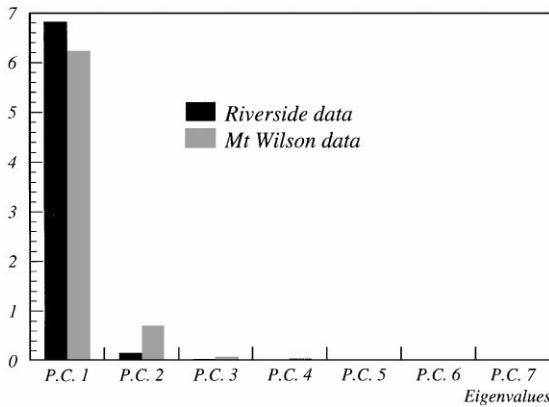


Fig. 9. Eigenvalues of the correlation matrices for Riverside and Mt Wilson.

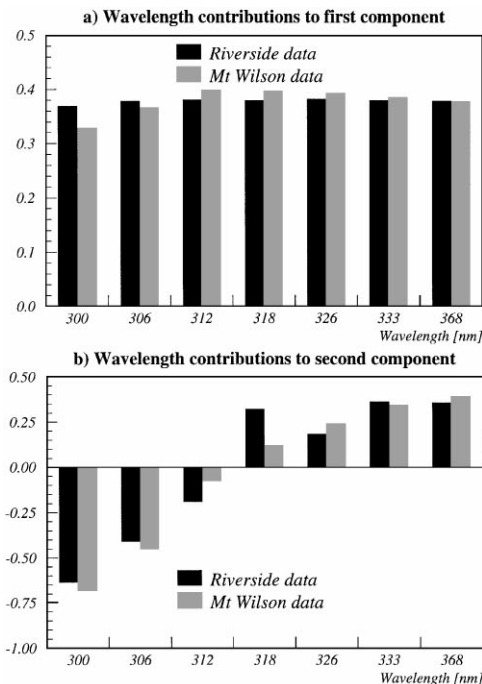


Fig. 10. Wavelength-dependent optical depth contributions to first and second principal components.

component signatures (the contribution to the components) at Riverside and Mt Wilson is an indication of the quality of the PCA discrimination. The only question mark is the 318-nm contribution to the second component at Riverside, but this component at Riverside is almost negligible.

At the observed wavelengths, principal component analysis suggests that almost all the optical depth variability is due to changes in aerosol concentration at both sites. At Riverside, the influence of aerosol variability is strong enough that the variability due to changes in

ozone column is negligible even at the shorter wavelengths. At Mt Wilson where the environment is more pristine, the optical depth variability is lower and the influence of changes in the ozone column is more influential, proportionally. When the aerosol and ozone variability are taken into account, the remaining unexplained variability is negligible (on the order of 1% or below).

Despite differences in component size at Riverside and Mt Wilson, the similarity of the principal component structure is remarkable. Similar physics are expected to be the cause of the variability in optical depths at Riverside and Mt Wilson; otherwise, there would be no reason for the wavelength-dependent optical depth contributions to the principal components to be similar at the two sites. This study shows that the most influential factors for the optical depth variability are the same (light absorption and scattering by aerosols as the major factor, and absorption by ozone as the minor factor), and are ordered in a similar fashion at the two sites. The study also quantifies the influence of each factor and indicates the differences in relative influence of aerosols and ozone on the variability associated with optical depth at Riverside and Mt Wilson.

It should be emphasized that this study focused on the variability associated with optical depth. Even though aerosol optical depth was found to be the most influential factor in the optical depth variability at all the wavelengths considered in this study, this does not imply that it is the most important contribution to the total optical depth. For example, it is possible that the variability in ozone optical depth occurs around a larger stable average value than for the aerosol. PCA would not extract the signal due to the stable average.

4. Conclusions

Using UV spectral irradiance data measured during SCOS97 at two California sites, we computed total optical depths and analyzed their variability during the four-month duration of the study. We have explored the temporal variability at two locations in a region with a long history of air pollution problems. We pointed out similarities between sites such as the overwhelming importance of changes in aerosol concentration in explaining the optical depth variability. We also pointed out the differences in optical depth resulting from higher air pollutant concentrations at Riverside: at this site, the optical depths and the optical depth variability are larger and the influence of factors other than aerosols is negligible in explaining the variability. At Mt Wilson, ozone column changes are non-negligible in explaining the variability. These conclusions are valid for clear-sky conditions. The presence of clouds can lead to large and rapid changes in the optical depth. Because of the

complexity of the issue, analysis of cloudy situations is beyond the scope of this study.

Since many characteristics of the atmosphere such as pollutant concentrations, broadband radiation, etc. were measured during SCOS97; it would be interesting to compare the results from this study with other results characterizing aerosol concentrations and ozone column. It would also be valuable to use optical depths derived here as input to a radiative transfer model and compare the results with NO₂ actinometric measurements that were made at the same time.

Acknowledgements

The authors thank Jim Pederson of CARB, Jim Gibson of CSU, Steve Reynolds of Envair, and Sasha Madronich of NCAR for their valued advice, and the reviewers for their constructive comments and suggestions.

This research was funded by the California Air Resources Board under Contract no. 96-335. The statements and conclusions in this paper are those of the authors, and not necessarily those of the California Air Resources Board.

References

- Baldasano, J.M., Delgado, R., Calbo, J., 1998. Applying receptor models to analyze urban/suburban VOCs air quality in Martorell (Spain). *Environmental Science and Technology* 32, 405–412.
- Bergin, M.S., Russell, A.G., Milford, J.B., 1998. Effects of chemical mechanism uncertainties on the reactivity quantification of volatile organic compounds using a three-dimensional air quality model. *Environmental Science and Technology* 32, 694–703.
- Bigelow, D.S., Slusser, J.R., 2000. Establishing the stability of multi-filter UV rotating shadowband radiometers. *Journal of Geophysical Research* 105, 4833–4840.
- Bigelow, D.S., Slusser, J.R., Beaubien, A.F., Gibson, J.H., 1998. The USDA Ultraviolet Radiation Monitoring Program. *Bulletin of the American Meteorological Society* 79, 601–615.
- Dickerson, R.R., Kondragunta, S., Stenchikov, G., Civerto, K.L., Doddridge, B.G., Holben, B.N., 1997. The impact of aerosols on solar ultraviolet radiation and photochemical smog. *Science* 278, 827–830.
- Everitt, B.S., Dunn, G., 1992. *Applied Multivariable Data Analysis*. Oxford University Press, New York.
- Falls, A.H., McRae, G.J., Seinfeld, J.H., 1979. Sensitivity and uncertainty of reaction mechanisms for photochemical air pollution. *International Journal of Chemical Kinetics* 11, 1137–1162.
- Gao, D., Stockwell, W.R., Milford, J.B., 1995. First-order sensitivity and uncertainty analysis for a regional-scale gas-phase chemical mechanism. *Journal of Geophysical Research* 100 (23), 23153–23166.
- Gao, D., Stockwell, W.R., Milford, J.B., 1996. Global uncertainty analysis of a regional-scale gas-phase chemical mechanism. *Journal of Geophysical Research* 101, 9107–9119.
- Harrison, L., Michalsky, J., 1994. Objective algorithms for the retrieval of optical depths from ground-based measurements. *Applied Optics* 33, 5126–5132.
- Henry, R.C., Hidy, G.M., 1979. Multivariate analysis of particulate sulfate and other air quality variables by principal components – Part I. Annual data from Los Angeles and New York. *Atmospheric Environment* 13, 1581–1596.
- Henry, R.C., Hidy, G.M., 1982. Multivariate analysis of particulate sulfate and other air quality variables by principal components – Part II. Salt Lake City, Utah and St. Louis, Missouri. *Atmospheric Environment* 16, 929–943.
- Jolliffe, I.T., 1972. Discarding variables in a principal component analysis 1: Artificial data. *Applied Statistics* 21, 160–173.
- Larson, S., Cass, G., Hussey, K., Luce, F., 1984. Visibility model verification by image processing techniques. Final Report to State of California Air Resources Board under Agreement A2-077–32, Sacramento, CA.
- Lean, J.L., Rottman, G.J., Kyle, H.L., Woods, T.N., Hickey, J.R., Puga, L.C., 1997. Detection and parameterization of variations in solar middle and near-ultraviolet radiation (200–400 nm). *Journal of Geophysical Research* 102, 29939–29956.
- Madronich, S., 1987. Photodissociation in the atmosphere 1. Actinic flux and the effects of ground reflections and clouds. *Journal of Geophysical Research* 92, 9740–9752.
- Meng, Z., Dabdub, D., Seinfeld, J.H., 1997. Chemical coupling between atmospheric ozone and particulate matter. *Science* 277, 116–119.
- Milford, J.B., Gao, D., Russell, A.G., McRae, G.J., 1992. Use of sensitivity analysis to compare chemical mechanisms for air-quality modeling. *Environmental Science and Technology* 26, 1179–1189.
- Odum, J.R., Jungkamp, T.P.W., Griffin, R.J., Flagan, R.C., Seinfeld, J.H., 1997. The atmospheric aerosol-forming potential of whole gasoline vapor. *Science* 276, 96–99.
- Schmid, B., Spyak, P.R., Biggar, S.F., Wehrli, C., Seckler, J., Ingold, T., Mätzler, C., Kämpfer, N., 1998. Evaluation of the applicability of solar and lamp radiometric calibrations of a precision Sun Photometer operating between 300 and 1025 nm. *Applied Optics* 37, 3923–3941.
- Schmid, B., Michalsky, J., Halthorne, R., Beauharnois, M., Harrison, L., Livingston, J., Russell, P., 1999. Comparison of aerosol optical depth from four solar radiometers during the fall 1997 ARM intensive observation period. *Journal of Geophysical Research* 104, 2725–2728.
- Schotland, R.M., Lea, T.K., 1986. Bias in a solar constant determination by the Langley method due to structured atmospheric aerosol. *Applied Optics* 25, 2486–2491.
- Seinfeld, J.H., Pandis, S.N., 1997. *Atmospheric Chemistry and Physics*. Wiley/Interscience, New York.
- Shaw, G.E., Reagan, B.M., Herman, B.M., 1973. Investigations of atmospheric extinction using direct solar radiation measurements made with a multiple wavelength radiometer. *Journal of Applied Meteorology* 12, 374–380.
- Slusser, J.R., Gibson, J.H., Bigelow, D.S., Kolinski, D., Disterhoft, D.P., Lantz, K., Beaubien, A., 2000. Langley method of calibrating UV filter radiometers. *Journal of Geophysical Research* 105, 4841–4849.

- Steele, H.M., Turco, R.P., 1997. Separation of aerosol and gas components in the Halogen Occultation Experiment and the Stratospheric Aerosol and Gas Experiment (SAGE) II extinction measurements: Implications for SAGE II ozone concentrations and trends. *Journal of Geophysical Research* 102, 19665–19681.
- Stephens, G.L., 1994. *Remote Sensing of the Lower Atmosphere*. Oxford University Press, New York.
- Thomason, L.W., Herman, B.M., Reagan, J.A., 1983. The effect of Atmospheric Attenuators with Structured Vertical Distributions on Air Mass Determinations and Langley Plot Analysis. *Journal of Atmospheric Science* 40, 1851–1854.
- Tomasi, C., Vitale, V., De Santis, L.V., 1998. Relative optical mass functions for air, water vapour, ozone, and nitrogen dioxide in atmospheric models presenting different latitudinal and seasonal conditions. *Meteorological and Atmospheric Physics* 65, 11–30.
- Vuilleumier, L., Harley, R.A., Brown, N.J., 1997. First- and second-order sensitivity analysis of a photochemically reactive system (a Green's function approach). *Environmental Science and Technology* 31, 1206–1217.
- Yang, Y.J., Stockwell, W.R., Milford, J.B., 1995. Uncertainties in incremental reactivities of volatile organic compounds. *Environmental Science and Technology* 29, 1336–1345.
- Yang, Y.J., Stockwell, W.R., Milford, J.B., 1996. Effect of chemical product yield uncertainties on reactivities of VOCs and emissions from reformulated gasolines and methanol fuels. *Environmental Science and Technology* 30, 1392–1397.